DTIP 2009 of MEMS & MOEMS 1-3 April, Rome, Italy

A Clover Shaped Silicon Piezoresistive Microphone for Miniaturized Photoacoustic Gas Sensors

C. Grinde[1], P. Ohlckers[1], M. Mielnik[2], G. U. Jensen[2], A. Ferber[2], D.T. Wang[2]
1)Vestfold University College, PO. Box 2243,N-3103 Tonsberg, Norway
2)SINTEF ICT, PO. Box 124 Blindern, N-0134 Oslo, Norway

***Abstract*-Here we present the design and modeling of a novel piezoresistive microphone designed for a photoacoustic gas sensor system. The microphone is fabricated using a novel process to enable DRIE etch through of membranes of multiple thickness.**

I. INTRODUCTION

The photoacoustic principle for measuring gas concentrations is well established. Current systems are larger and more expensive than what is necessary. In this paper we present the design, modeling and fabrication of a dedicated silicon MEMS microphone for a miniaturized photo acoustic CO_2 gas sensor system. The microphone is a perforated membrane which resembles a four leaf clover supported by four beams with piezoresistors at their base. The microphone is processed in the MultiMEMS foundry process with intermediate processing at SINTEF MiNaLab in special customized add-on process allowing DRIE etch through membranes with varying thickness. Simulations indicate a sensitivity of 790µV/V Pa, which is a 71 times improvement compared to a clamped circular membrane microphone fabricated in the same MPW service [1].

II. PHOTOACOUSTIC GAS SENSORS

Gas sensors based on the photoacoustic principle are commercially available. Miniaturization using micro machined components will reduce costs and enable localized sensing of i.e. CO_2 concentrations in ventilation systems. The sensor principle is illustrated in Fig. 1. A pulsed Diamond-Like Carbon IR source operating between 20 and 100 Hz[2] emits light which is absorbed by the gas who's concentration is to be measured in the ventilated chamber. The transmitted light will enter a reference chamber filled with the gas of interest, where more light is absorbed. Whatever is not absorbed, reach a thermopile which provides means of compensation for non ideal effects such as aging and dirt. When absorbed, the pulsed light will increase entropy in the reference chamber, which results in an acoustic signal with the same frequency as the IR source. The acoustic amplitude is inversely proportional to the CO_2 concentration in the absorption path and can hence be measured with a microphone. While for macroscopic systems, one can use acoustic resonance in the reference chamber to increase the signal strength, this is not possible with the current IR sources available and the price- and size- range one is aiming for. A highly sensitive microphone is therefore required.

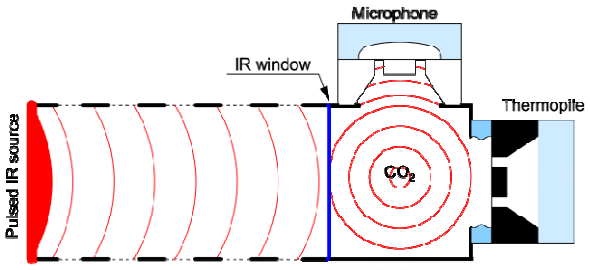

Fig. 1 Outline of the sensor system. A pulsed IR source emits IR light through a ventilated chamber. At the opposite end of the chamber sits a reference chamber. The intensity of the inbound IR light is proportional to the $C0_2$ concentration in the ventilated chamber. In the reference chamber, the light is absorbed as heat, which in turn leads to thermal expansion and pressure increase of the gas. The thermal expansion leads to an acoustic signal, whose amplitude is inversely proportional to the CO_2 concentration in the absorption path. The acoustic signals amplitude, and hence $C0_2$ concentration can be monitored using a microphone.

III. MICROPHONE

The silicon microphone we present here is a membrane with perforations along its' edges and suspended by four beams centered at each side. To maximize the surface area, while fitting the sensor inside the predefined die sizes from the MPW service [3] used, the beams are embedded inside the membrane area. The resulting geometry resembles a four leaf clover with beams attached between its' leafs. A top view of the geometry is illustrated in Fig 2. The rounded rectangles indicate regions of thin (3.1 µm) thickness while the rest of the membrane is thick (23µm). As can be seen in the formulas in 'Analytic model', the desired shape of these slots are deep and narrow to maximize the pressure difference over the membrane for the range of frequencies of interest [20-100Hz]. These slots are illustrated to the left in Fig. 3 for the cross section along A-A of Fig. 2.

IV. PIEZORESITIVE READOUT

The conversion from displacement to electrical signal is done using four piezoresistors at the base of the supporting beams as illustrated in Fig. 2. To maximize output and minimize temperature effects, the piezoresistors are configured in a full Wheatstone bridge with transverse and longitudinal resistors diagonal in the bridge(See Fig. 4).

 ISBN: 978-2-35500-009-6

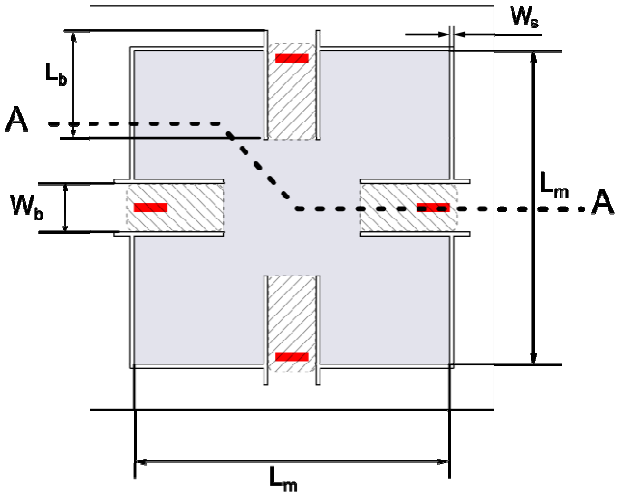

Fig. 2 Top view illustration of microphone membrane and suspension structures. Gray area in the centre correspond to thick regions while hatched areas correspond to thin beam regions. Surrounding the membrane region is a slot of width w_s. The red rectangles located on the base of the beam illustrate the piezoresistors and their orientations.

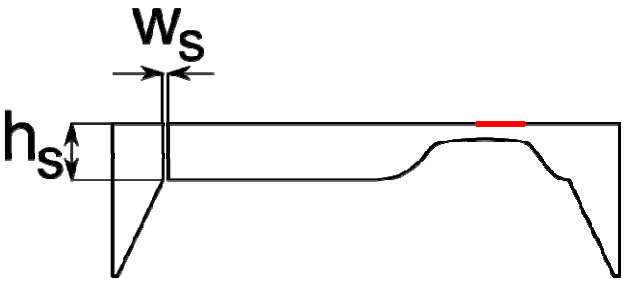

Fig. 3 Cross section profile of along A-A in Fig. 2. w_s and h_s are the slot width and height respectively.

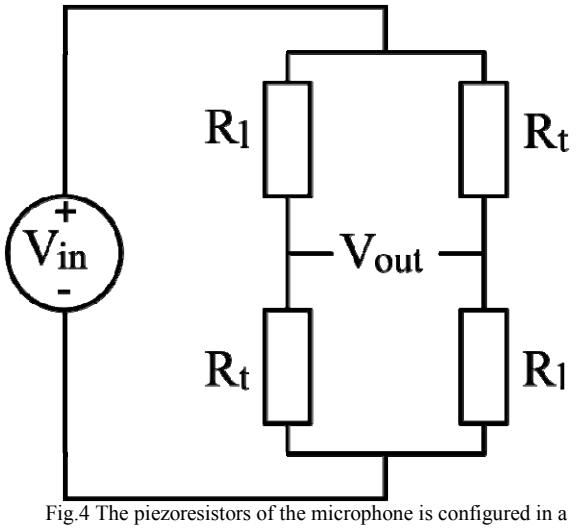

Fig.4 The piezoresistors of the microphone is configured in a Wheatstone bride to minimize temperature effects and maximize sensitivity

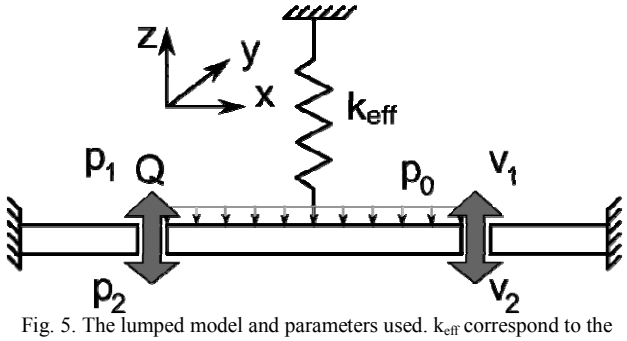

Fig. 5. The lumped model and parameters used. k_{eff} correspond to the combined stiffness of the four double clamped beams, Q to the gas flow, p_0 to the pressure difference p_1-p_2. The model is based on the assumption that the ventilation slot length into the drawing (y) is much larger than the length in the z direction.

V. Sensitivity Analysis

The acoustic amplitude is expected to be within the range of a linear model (p<< 1 Pa). Hence can we use linear models when analyzing the sensitivity.

A. Mechanical Domain

For mechanical domain the membrane and its suspension can be described using the equations of motion

$$m\,x + c\,\dot{x} \ddot{+} kx = F \qquad (1)$$

where m, c and k are the mass, damping coefficient and equivalent stiffness of the supported membrane. F is the sum of forces applied to the system. The $\ddot{x}$ and $\dot{x}$ refer to the second and first order time derivative of the displacement x. The mass can easily be found as the volume multiplied with density. The damping coefficient of the material itself can be disregarded as the intrinsic damping in single crystal silicon is very small compared to gas damping. For the equivalent stiffness of our four beam system, we assume the center membrane is infinitely stiff compared to the supporting beams. The lumped effective stiffness, as featured in Fig. 5, can be the be found as four times the stiffness of one double clamped beam of length L, thickness t and width w [7]

$$k_{eff} = 4\frac{12\,Ey\,Iy}{{L_{beam}}^3} \qquad (2)$$

With both the second area moment Iy(x) and the beam thickness t(x) being functions of position (see Fig. 6) along the beam, the surface stress can be found as

$$\sigma = M_b/(I_y\,(x)\,)\,\frac{t(x)}{2} \qquad (3)$$

where Mb is the bending moment from the forces applied to one beam. For a double clamped beam, the bending moment at location x with a load F at one end is

$$M_b = \frac{F\,(L_b - x)}{2} \qquad (4)$$

The models listed in [7] and given in (2) is based on the assumption of uniform thickness along the length of the beam, so our model based on beams with a varying thickness, is checked vs. FEA.

 ISBN: 978-2-35500-009-6

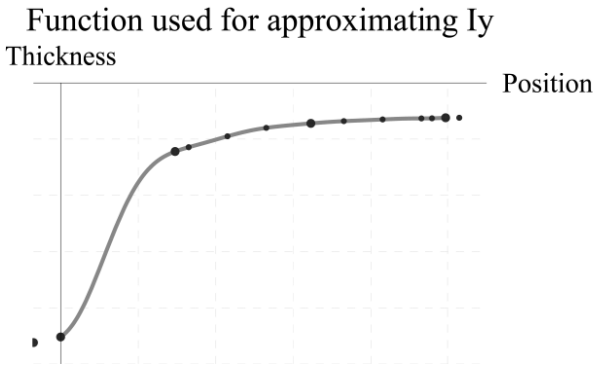

Fig. 6 The polynomial used to approximate the shape of the soft transition region stemming from the fabrication process. The large dots indicate the information provided by the MPW service while the smaller dots are the interpolation points that are used in addition to the given points. Axis values are obtainable from [3].

B. *Coupled model*

Due to the small dimensions in the direction of wave propagation compared to the wavelengths in the frequency range of interest (20Hz < f <100 Hz), the system can be considered as a pressure-structure interaction rather than an acoustic-structure interaction. Estimation for the flow velocity through the ventilation slots shows that it is much smaller than the speed of sound in air, which is about 343 m/s at room temperature. We can therefore consider the gas as incompressible. The acoustic domain can therefore be reduced to a quasi static model.

We now make two assumptions: The backside of the microphone is open to an infinite large volume at ambient pressure, and the volume which the pressure is generated is sufficiently large to not be effected by the volume that passes through the membrane slot during one half cycle. With reference to the lumped model in Fig. 5: The first assumption allows us to use p_2 as a reference pressure, meaning p_2=0. The second assumption allow us to consider p_1 as absolute to p_2, leaving p_0 to equal the combination of p_1 and the dynamic pressure. The forces in (1) can now be found by multiplying the area of the membrane with the pressure difference over the membrane. We can now use the stagnation pressure for the effective pressure

$$p_0(t) = p_1(t) + \frac{1}{2}\rho v^2 \qquad (5)$$

Here v is the flow velocity through the slot and ρ is the density of the gas. Assuming no slip conditions along the walls of the slot channel, the flow rate can be expressed as [6]

$$Q = \frac{1}{12}\frac{w_s{}^3\, L\, p_0(t)}{\eta\, h_s} \qquad (6)$$

We can now find the average flow velocity v by dividing (6) with the opening area of the channel. Combining (1), (5) and (6), we can express the equation governing the displacement of the suspended diaphragm as

$$m\ddot{z} + b\dot{z} + kz = A_m(p_0) \qquad (7)$$

with A_m as the membrane area. As the membrane moves, the effective length of the slot will change, which is included in the model via the expression for average flow velocity through the slot

$$v = \frac{w_s{}^3}{12\eta(h_s - |z|)^2} p_1(t) \qquad (8)$$

If we assume a harmonic varying pressure, we can express the pressure in the reference chamber as

$$p_1(t) = p_1 \sin(\omega\, t) \qquad (9)$$

where ω and t are the angular frequency and time respective. p_1 is the semi-amplitude of the pressure, meaning the pressure vary between $\pm p_1$ through one full cycle.

VI. ANALYTIC RESULT

A. *Mechanical model*

The mechanical model has been implemented in Mathematica 7 and verified using the FEA software ANSYS 11. To compare the models, a static pressure of 1 Pa was applied to both models. Data were extracted along the top surface along the centre of the beam, corresponding to the leftmost edge of the bent beam section in Fig. 7. To minimize computational effort, only one eight of the structure was simulated. Fig. 8 shows a comparison of surface stress along the top surface of the beam between the analytic model and the results from the FEA. The analytic model underestimate the FEA results by less than 15% for the geometry and mesh used.

B. *Coupled model*

The coupled model has been implemented in Mathematica 7.0 and solved numerically using the geometries for the sensor described above, pressure semi-amplitude of 1 Pa and initial displacement and velocity set to zero. The damping coefficient *b* from (5) is assumed negligible. Using the viscosity and density for air at room temperature, the resulting steady state amplitude is extracted and plotted vs. frequency for the range of frequencies the

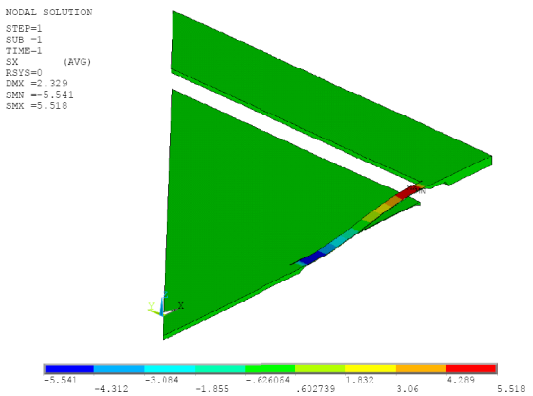

Fig. 7. FEA results showing stress in MPa along the length of the supporting beam when the membrane is subject to 1 Pa static pressure. Legend show a maximum stress of 5.54 MPa and a displacement of 2.32μm.

 ISBN: 978-2-35500-009-6

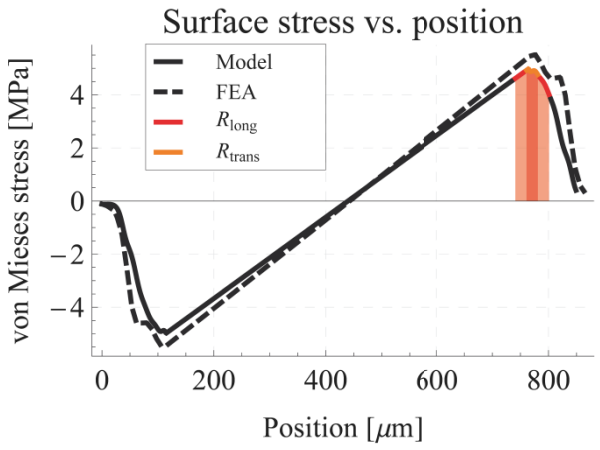

Fig. 8. The analytical model has been verified using FEA. The figure shows stress extracted along the centre of the beam compared to the surface stress profile from the analytical model, when the microphone is subject to 1 Pa static pressure. The colored regions correspond to the position and extent of the longitudinal and transverse resistors.

solide state IR source[2] can operate at in Fig. 9. Note that in the model, the frequency dependent performance of the IR source is not accounted for, so for the full sensor system, the frequency response will differ from the results presented here. The analytic model shows amplitude that increase linearly with frequency for the microphone. For the low range of frequencies, the peak to peak amplitude is about two times the static deflection from Fig. 7.

VII. Verification and Qualification

The analytic model for the mechanical domain has been verified using ANSYS FEA software and a one-eight symmetry model as seen in Fig. 5. The same FEA model was used to qualify the design for production at the MPW service provider [3]. This involved simulation of 1 bar pressure over the membrane prior to etch through and 2000 g acceleration in any direction after etch through. Both load cases are outside the range for the analytical model due to complexity and nonlinearities.

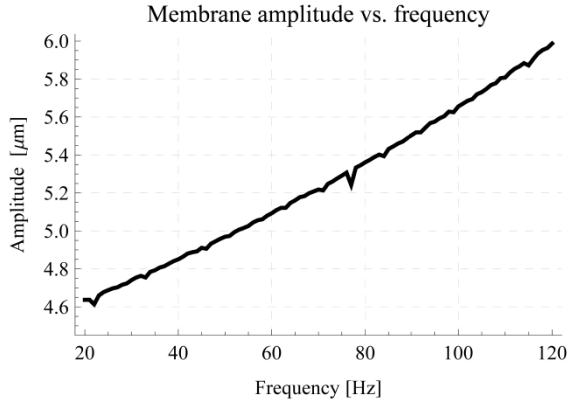

Fig. 9. Membrane peak to peak amplitude vs. frequency for the frequency range for which the IR source [2] can operate. For all frequencies, a pressure amplitude of 1 Pa is used and the viscosity for air at room temperature. The frequency dependent performance of the IR source is not accounted for.

Fig. 10. A typical cross section for a device fabricated in the MultiMEMS process.

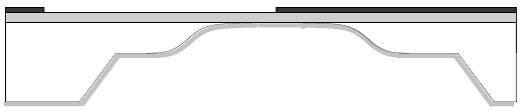

Fig. 11 Aluminum is sputtered on the backside and resist deposited and patterned on the front side.

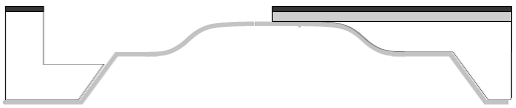

Fig. 12 DRIE is used to etch 100 microns down, terminating against the backside aluminium if thinner regions are etched.

Fig. 13. Aluminum is stripped to release the structure.

VIII. Fabrication

The microphone has been fabricated using the MPW service MultiMEMS from SensoNor Technologies [3]. The process offered by MultiMEMS is a silicon bulk micromachining process using electrochemical passivation of n-regions to form high precision thickness membranes of two thicknesses: 3.1 and 23 µm. A detailed process description is given in [3]. The process offers the possibility of piezoresistors and conductors at two depths, and a DRIE release etch offering perforation and recesses to a nominal depth of 10 µm, which for this design, is not used. Instead a custom process offered as an add-on process by SINTEF MiNaLab in the EU funded project microBUILDER[5], has been used.

A. Custom processing

The custom process used enable DRIE etch through regions of 3 µm and 23 µm thickness in one single operation. After the backside etching with electrochemical passivation of the n-regions [4], a cross section of a typical device fabricated in the MultiMEMS process will have regions of varying thicknesses as illustrated in Fig. 10. To act as a termination layer for the DRIE, aluminum is sputtered on the backside of the wafer, before resist is deposited and patterned on the front side (Fig. 11). DRIE is then used to etch to either 100 µm depth or to terminating against the aluminum (Fig. 12). The final step of the additional processing is to strip the aluminum on the backside (Fig. 13) before the wafers are put back into the normal MultiMEMS process, where anodic bonding of glass on both sides follows. The finalized die consists of a glass-silicon-glass structure as pictured in Fig. 14. A top view micrograph is included in Fig. 15. The circle in the center is the top glass hole, while the oddly shaped dark regions are the remains from help structures used during the backside

 ISBN: 978-2-35500-009-6

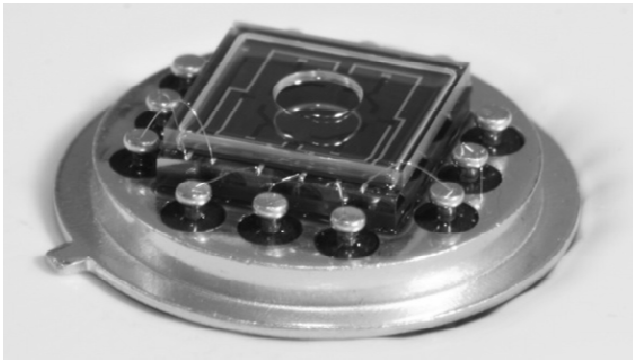

Fig. 14. Finished microphone mounted in a TO 8 package and wire bonded. Die size is 6 x 6mm^2.

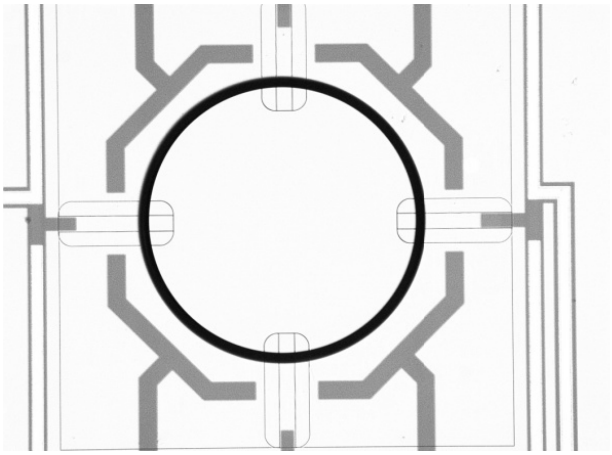

Fig. 15 Top view of microphone. Circle in the centre is hole in glass as seen in Fig. 22. Rectangles with rounded corners at the membrane perimeter is 3 micron thick areas with dark areas indicating the position of the piezoresistors. Other dark a.

etching step. At the base of the beams, surrounded by rectangles with rounded corners, are darker regions of surface oxide, protecting the underlying piezoresistors from surface pollution. The two parallel lines through the rounded rectangles are the slots that define the width of the beams. Springing out from the base of the beam are the slots that define the perimeter of the beams. A more detailed image of the base of one beam is included in Fig. 16.

IX. Results and Summary

A novel microphone structure has been designed, modeled and fabricated. Images of the finished device re included in figures 14, 15 and 16. Results from the analytical and FEA models indicate a sensitivity of 0.79 mV/V Pa for the frequency range of interest [20 to 100 Hz]. This is a 71 times improvement compared to the design in [1] which is fabricated in the same process with no additional post processing.

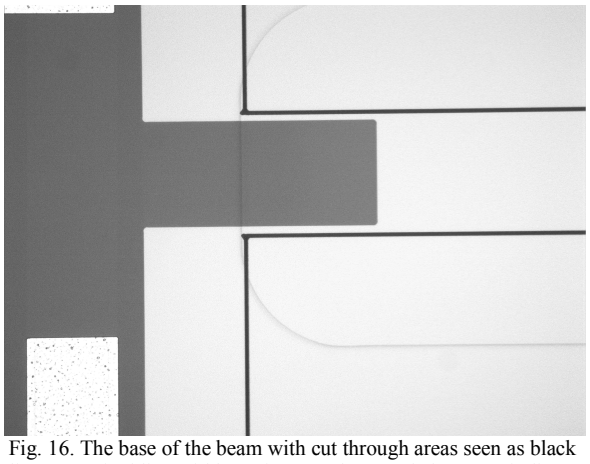

Fig. 16. The base of the beam with cut through areas seen as black lines. Nominal line width 3 microns. The rounded corners indicate the position transition from thick to thin membrane.

Coupled FEA models are currently being implemented to verify the analytical coupled model. Characterization of the sensor is work in progress.

Acknowledgment

The device fabrication processing has been sponsored by Sensonor technologies and the additional postprocessing performed at SINTEF MiNaLab and financed by The Research Council of Norway through project no. 181712/I30: "Microtechnological research platform".

References

[1] Schjolberg-Henriksen, K.; Wang, D.; Rogne, H.; Ferber, A.; Vogl, A.; Moe, S.; Bernstein, R.; Lapadatu, D.; Sandven, K. & Brida, S. 'High-resolution Pressure Sensor for Photo Acoustic Gas Detection', Sensors and Actuators A: Physical, The 19th European Conference on Solid-State Transducers, 2006, 132, 207-213

[2] P. Ohlckers, T. Skotheim, V. Dmitriev, G. Kirpilenko : "Advantages and Limitations of Diamond-Like Carbon as a MEMS Thin Film Material" Technical Proceedings of the 2008 NSTI Nanotechnology Conference and Trade Show 2008, Volume 1, Chapter 1: Carbon Nano Structures & Applications, pp. 63-66.

[3] MultiMEMS design handbook v. 4.1 . Can be obtained via http://www.multimems.com

[4] Kloeck, B.; Collins, S. D.; Derooij, N. F. & Smith, R. L., "Study of Electrochemical Etch-stop for High-Precision Thickness Control of Silicon Membranes.", IEEE Transactions on Electron Devices, 1989, 36, 663 – 669

[5] MicroBuilder design hand book V2. Can be obtained via http://www.microbuilder.org

[6] Henrik Bruus ,"Theoretical Microfluidics"ISBN13: 9780199235094,ISBN10: 0199235090,Oxford University press,2007

[7] Roarks Formulas for stress and strain. McGraw-Hill, 2002